Applied Mathematical Modelling 131 (2024) 487–504

Contents lists available at ScienceDirect

Applied Mathematical Modelling

journal homepage: www.elsevier.com/locate/apm

Computational modeling of microalgal biofilm growth in heterogeneous rotating algal biofilm reactors (RABRs) for wastewater treatment

Gerald Benjamin Jones [a], Ronald C. Sims [b], Jia Zhao [c,*]

[a] Department of Mathematics and Statistics, Utah State University, 84322, United States of America
[b] Department of Biological Engineering, Utah State University, 84322, United States of America
[c] Department of Mathematics and Statistics, Binghamton University, 13902, United States of America

A B S T R A C T

Rotating algal biofilm reactors (RABRs) are innovative systems designed to cultivate microalgae biofilms efficiently. In this paper, we have developed a novel mathematical model to accurately capture the growth dynamics of algae biofilms within RABR. By considering the spatial heterogeneity of the RABR, we introduce a PDE-based model that addresses the spatial variations across the substratum, enabling a more accurate simulation of biofilm growth in RABRs. The photosynthesis process is modeled through reactive kinetics, driving the growth of the algae biofilm. To analyze the system's behavior, we employ finite difference numerical methods to solve the complex PDE model. We then conduct extensive numerical simulations to understand algae biofilm growth in the RABR environment under various operational factors and environmental conditions. One primary focus in these simulations is to investigate the impact of various harvesting strategies, harvesting frequencies, light intensity, and light exposure on the overall biomass productivity of the algae biofilm. The numerical results provide valuable insights into optimizing algae biofilm growth and designing harvesting techniques in RABR systems. Our proposed novel mathematical model provides an effective platform for the theoretical investigation and design of RABRs for wastewater treatment.

1. Introduction

The study and cultivation of microalgae have become a critical component in sustainably addressing the multifaceted environmental obstacles of the 21st century, especially in wastewater treatment. Microalgae are highly effective at removing pollutants such as nitrogen and phosphorous from wastewater while also producing valuable biomass that is utilized for biofuel production, animal feed, agricultural fertilizers, bioplastics, as well as pharmaceuticals and nutraceuticals [1–5]. Traditionally, microalgae have been cultivated in suspended cultures (remaining in a liquid medium), such as open ponds and photobioreactors. These suspended culture systems were favored due to their simplicity and low initial costs. However, these suspended systems also face challenges in enhancing biomass production as they usually require continuous aeration and mixing to prevent sedimentation and ensure uniform light exposure. Suspended systems also suffer from low light utilization efficiency and high water evaporation rates [6].

In response to these limitations, the exploration of microalgae biofilms, a mixture of microalgae and biofilm colonies, has emerged as a promising alternative. Instead of planktonic bacteria, biofilms are a collection of bacteria and glue-like extracellular polymeric substances (EPS) that are usually attached to a substratum. The microalgae biofilm offers a structured medium that can overcome many of the limitations of suspended cultures. Among various microalgae biofilm cultivation technologies, the rotating algae biofilm reactor (RABR) system has attracted noticeable attention in the past decade [7–9]. The RABR cultivates microalgae biofilms on a

* Corresponding author.
E-mail address: jzhao10@binghamton.edu (J. Zhao).

https://doi.org/10.1016/j.apm.2024.04.021
Received 9 May 2023; Received in revised form 25 March 2024; Accepted 8 April 2024

Available online 12 April 2024

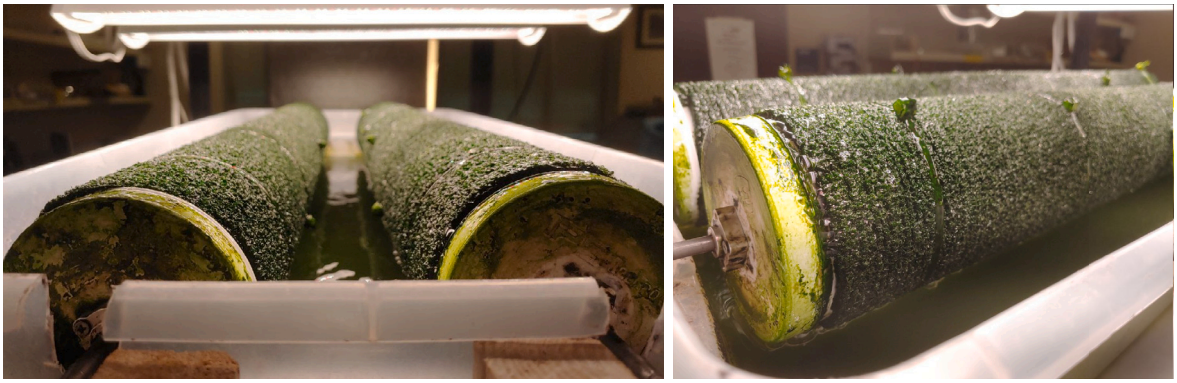

Fig. 1. A side view of the laboratory scale RABRs operating at the USTAR Bioinnovations Center in Logan, Utah. The algae biofilm is grown on a polyethylene substratum sheet and rotated into a 40 L tank containing anaerobic digester effluent.

rotating surface that periodically immerses the algae biofilm in nutrient-rich media and exposes it to air and light. This dynamic environment optimizes the exposure of the biofilm to essential growth factors, significantly enhancing biomass productivity and operational efficiency compared to traditional suspended culture methods. Notable bioproducts from RABR systems include bioplastic, phycocyanin, biofertilizer, biodiesel, biocrude, and dietary protein [10–15], highlighting their versatility and potential in bioinnovation.

Despite these advantages, optimizing RABR systems for maximum biomass productivity and nutrient uptake requires an in-depth understanding of various operational parameters, such as water pH, the reactor's rotation speed, the duty cycle of immersion and exposure, hydraulic retention time, and harvesting strategies (including harvesting frequency and harvesting percentage), in addition to the environmental conditions, such as the temperature and the photosynthetic photon flux density (PPFD) which measures the amount of light available for photosynthesis, with units of μmol of photons per square meter per second, i.e., $\mu\text{mol}/(m^2 s)$. The influence of PPFD on biofilm growth varies across different light regimes and potentially leads to photosynthesis inhibition at high intensities. Traditional experimental approaches are limited in exploring these operational and environmental factors due to their practical challenges.

Mathematical modeling offers a powerful and cost-effective approach for exploring the interplay between operational and environmental factors that eventually provide insights into the design, optimization, and scale-up of RABR systems. Early models have primarily focused on homogeneous microalgae growth in response to homogeneous factors, such as light intensity and temperature, CO_2, and nutrient concentrations, and therefore use dynamical systems without spatial variability [16]. Given the critical role of light for photosynthesis in determining microalgae biofilm growth, recent modeling advances have included PPFD/light and its attenuation within biofilms (light intensity decays during its penetration into the microalgae biofilm layers). Models that utilize PPFD as the key indicator for biofilm growth usually identify three distinct light conditions [17,18]: (1) a photosynthesis regime constrained by insufficient PPFD, (2) a regime where photosynthesis reaches saturation due to sufficient PPFD, and (3) an inhibited regime where excessive PPFD leads to photoinhibition. The initial models taking the impact of PPFD into account usually assume that the photosynthetic activity across the entire culture is influenced by the interaction between incident light and the entire culture. Such phenomenological models have evolved into various forms based on Monod-like relationships, Poisson distributions, and hyperbolic tangent functions [19–21]. More sophisticated models have considered the heterogeneity of light exposure by utilizing Beer-Lambert's law [22] to better represent light attenuation and its effects on biofilm productivity [18].

Despite the many existing models for microalgae biofilm growth, there is a lack of models tailored specifically for RABRs, which feature unique operational and environmental interactions that are distinct from traditional microalgae cultivation systems. These include the rotational movement influencing light exposure and nutrient distribution, the specific microalgae biofilm thickness affecting photosynthetic efficiency, the shear forces acting on the microalgae biofilm, and the spatial heterogeneity of the RABR, as well as the harvesting microalgae biofilms off the substratum. Fig. 1 showcases a pair of laboratory-scale RABRs (40L) operating at the Utah Science Technology and Research Initiative (USTAR) Bioinnovations Center in Logan, Utah, for nutrient removal and biomass feedstock for biofuel, bioplastic, and biofertilizer production. It represents a physical model of a microalgae-based biofilm reactor for wastewater reclamation. Additionally, Fig. 2 presents a pilot scale RABR operating at the Central Valley Water Reclamation Facility (CVWRF). Customized models for RABRs would enable a more precise understanding of the interplay between operational parameters and environmental conditions, ultimately providing insights to enhance nutrient uptake efficiency and algae biomass productivity. Some seminal work on customized microalgae biofilm models for RABRs includes [17,18,23–25].

However, all the existing works oversimplify the RABR by neglecting its spatial heterogeneity. These models typically assume uniform conditions across the RABR, overlooking variations in light intensity, nutrient availability, and biomass concentration across the RABR that would impact growth rates and productivity. This study, built upon these existing customized RABR models, aims to fill this gap by developing a novel mathematical model that incorporates spatial heterogeneity within RABR systems and investigates the impact of spatial heterogeneity of the RABR system on biomass productivity and nutrient uptake under various operational

Fig. 2. A side view of the pilot scale RABR operating at the Central Valley Water Reclamation Facility (CVWRF). The algae biofilm is grown on a square substratum sheet and rotated into a 4,500 L tank containing anaerobic digester effluent. A plastic polycarbonate cover has been mounted to reduce heat loss in the winter months.

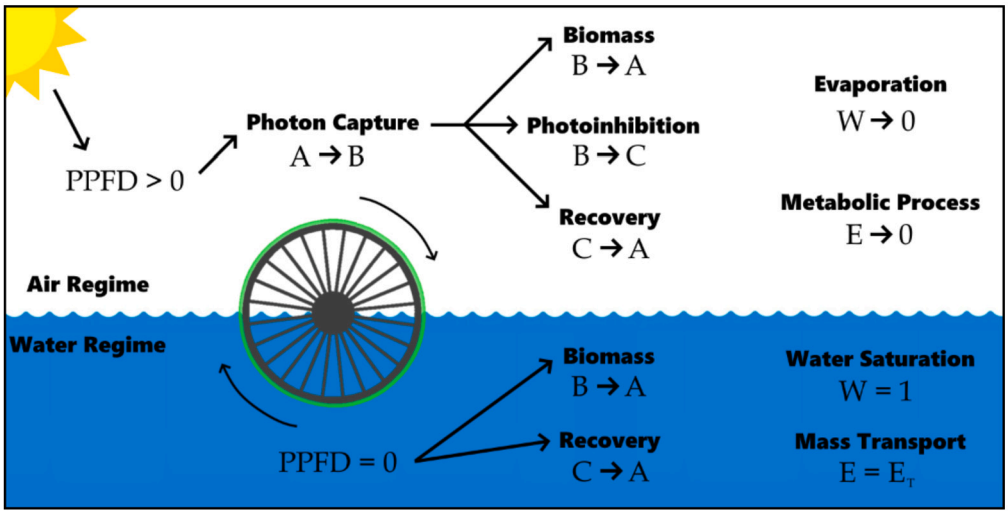

Fig. 3. A schematic illustration of the rotating algal biofilm reactor (RABR) and the photosynthetic system. This figure illustrates the proposed computational model for the RABR. Here, we use A, B, and C to represent the reactive, activated, and inhibited states, respectively.

and environmental conditions. Specifically, this work builds upon and significantly extends our previous work [25] by introducing a spatial resolution of the RABR into algae biofilm modeling to highlight the spatial variations across the RABR substratum. This enables more accurate modeling of biofilm growth in RABRs for situations that include various harvesting strategies and heterogeneous light exposure and penetration. With the model, we conduct an intensive numerical study in non-uniform environments affecting the algae biofilm and investigate the effects of various RABR operating and environmental factors on the algae biofilm growth and productivity.

2. Mathematical model formulation

In this section, we present a comprehensive derivation of the mathematical model for microalgae biofilm in the RABR. The microalgae biofilm growth could be effectively captured with a photosynthetic system due to the pivotal role of light in driving algae biofilm productivity. Drawing on the photosynthetic system model proposed by [17], we describe the reactive kinetics within algae biofilms through three cellular states: reactive, activated, and inhibited. In this model, cells in the reactive state are primed for photon absorption, transitioning to the activated state, where solar energy is converted into chemical energy for biofilm growth. Excessive solar radiation can shift cells from the activated state to the inhibited state, rendering them dormant. Fig. 3 visually summarizes this process and illustrates the cyclical exposure of the algae biofilm to aqueous and aerial environments within the RABR system.

In this paper, the algae biofilm is treated as a single species for simplicity and clarity in modeling the biomass productivity in RABR across different environmental and operational conditions. However, for a model that more accurately reflects the complex

biological nature of algal biofilms, it is necessary to consider the distinct roles and interactions of bacteria, EPS, and algae [26]. While the current model adopts a simplified approach to focus on the fundamental growth dynamics, our future research will incorporate these additional biological components and their interactions.

2.1. Photosynthetic kinetics with spatial heterogeneity

Consider a substratum with length L. We introduce the spatial variable x, $0 \le x < L$, to represent the spatial location of the substratum. We use $A(x,z,t)$, $B(x,z,t)$ and $C(x,z,t)$ to represent the fractions of A, B, C states at location x and height z, where $z \in [0, h(x,t)]$ and $h(x,t)$ represents the thickness of biomass at location x and time t. The photosynthetic reactive-kinetic model [17,18] can be extended as

$$\partial_t A(x,z,t) = D_a A_{xx} - \sigma I(x,z,t)A(x,z,t) + \frac{B(x,z,t)}{\tau} + k_r C(x,z,t), \tag{1a}$$

$$\partial_t B(x,z,t) = D_b B_{xx} + \sigma I(x,z,t)A(x,z,t) - \frac{B(x,z,t)}{\tau} - k_d \sigma I(x,z,t)B(x,z,t), \tag{1b}$$

$$\partial_t C(x,z,t) = D_c C_{xx} - k_r C(x,z,t) + k_d \sigma I(x,z,t)B(x,z,t), \tag{1c}$$

where $x \in [0, L)$, $z \in [0, h(x,t)]$, and D_a, D_b, and D_c denote the passive transport among the states A, B and C, respectively. The function $I(x,z,t)$ specifies the light intensity within the biofilm at any given point and time. The transition rates between these states are governed by k_r, the rate at which cells repair from the inhibited state C back to the reactive state A; k_d, the rate of damage transition from the activated state B to the inhibited state C under high light intensity; τ, the turnover time of the electron transport chain, and σ, the effective absorption cross-section per unit of photosynthetic units. Readers are encouraged to refer to [17,18] for a more comprehensive understanding of the photosynthetic process and its modeling.

Due to the incompressibility, we have the constraint

$$A(x,z,t) + B(x,z,t) + C(x,z,t) = 1, \quad \forall (x,z,t) \in [0,L] \times [0, h(x,t)] \times [0,T],$$

which leads to the constraint

$$\partial_t \Big[A(x,z,t) + B(x,z,t) + C(x,z,t) \Big] = 0.$$

Adding the terms in eq. (1) leads to

$$D_a A(x,z,t)_{xx} + D_b B(x,z,t)_{xx} + D_c C(x,z,t)_{xx} = 0,$$

which are the constraints on choosing the model parameters. For simplicity, we assume that $D_a = D_b = D_c$ in this paper.

2.2. Light exposure within RABR

The substratum undergoes periodic exposure to sunlight and water as the RABR rotates, with a portion submerged in water and the rest exposed to sunlight. The substratum length, denoted as L, and the length exposed to the air, denoted by l_*, are pivotal to the dynamics of light exposure within the RABR. With the RABR rotating, the relation between the RABR's peripheral velocity (v), its circumference (L), and the rotation period (T) is given by $T = \frac{L}{v}$.

Since the substratum forms a closed loop, the spatial variable could be defined in real space with a period of L. Define the flag function

$$\Gamma(x,t) = f\Big(\mathrm{mod}(x + vt, L)\Big), \quad f(x) = \frac{1}{1 + e^{-\frac{x-(1-r_0)L}{\epsilon}}}, \tag{2}$$

where $f(x)$ is the logistic function with ϵ a parameter controlling the transition thickness of the S-shape curve, and $r_0 := \frac{l^*}{L}$ is the ratio of substratum exposure to the air. In this paper, we set $\epsilon = 0.1$ fixed for simplicity. The function $\Gamma(x,t)$ performs as the flag function to mark whether the location x at time t is exposed to the air ($\Gamma(x,t) = 1$) or submerged ($\Gamma(x,t) = 0$). Namely, we have assumed that the biomass is either in fully bright or dark condition. We note that, under natural conditions, the sunlight intensity reaching the algae biofilm would be influenced by the sun's angle. This feature could lead to varying light penetration, which will be considered in our later study.

Furthermore, we model the actual light intensity by a square wave defined as

$$\hat{I}(x,t) = \hat{I}_0(t)\Gamma(x,t), \tag{3}$$

with $\hat{I}_0(t)$ the peak light intensity. To approximate $\hat{I}_0(t)$, we utilize existing light intensity data on April 25th, 2018, collected from the Sustainable Waste to Bioproducts Engineering Center (SWBEC) in Utah. The light intensity is measured as photosynthetically active radiation (PAR) every 15 minutes for 24 hours. We then fit the PAR data with a smooth function $\hat{I}_0(t)$ as shown in Fig. 4 for a range of one day. Moreover, we let $t = 0$ within our simulations correspond to 8:00 AM, and we assume each day has the same light pattern when simulating for a more extended period in this paper.

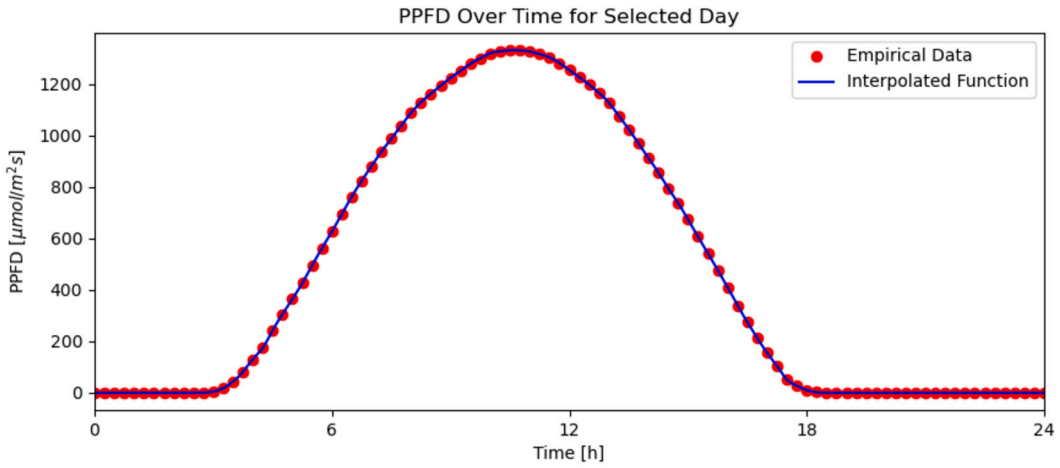

Fig. 4. Light intensity $\hat{I}_0(t)$ over time. The figure illustrates 24-hour PAR data as red points, with a fitted continuous function represented by a blue curve. This continuous function will be employed for subsequent simulations, starting at $t = 8$ hours for the interpolated function within the model for simulations.

Incorporating algae biofilm thickness necessitates establishing a connection between light attenuation and algae biofilm depth. Intuitively, the accessible light for each cell's photosystem diminishes as getting deeper into the algae biofilm. We model this relationship by adopting Beer-Lambert's law [18]. The light intensity $I(x,z,t)$ at time t, location x and depth z can be expressed as

$$I(x,z,t) = \hat{I}(x,t)e^{-b(h-z)}, \quad x \in [0,L] \quad z \in [0,h(x,t)], \tag{4}$$

where $\hat{I}(x,t)$ is defined in eq. (3), and b is a constant denoting the light attenuation factor.

2.3. Nutrient uptake mechanism

For algae biofilm to accumulate biomass, it must regularly access adequate nutrients, absorbed through nutrient mass transport. Nutrients could include phosphorous or ammonia. To simplify the model, we assume the nutrient concentration, $E(x,z,t)$, is uniform across different algae biofilm depths, thus simplifying E to depend only on substratum location x and time t. Hence, $E(x,t)$ represents the average nutrient concentration at location x and time t in the RABR, disregarding the algae biofilm thickness, while $E_T(t)$ denotes the average nutrient concentration in wastewater where the nutrient distribution, assumed to be spatially homogeneous.

Considering the finite availability of nutrients in the air, the uptake rate depends on the algae biofilm mass and the portion converting to biomass in state B. Meanwhile, nutrient levels are replenished when the biofilm is submerged in water. The nutrient dynamics are governed by

$$\partial_t E(x,t) = D_E E_{xx} - \frac{\gamma_{a1} E(x,t)}{K_a + E(x,t)} \int_0^{h(x,t)} B(x,z,t)dz - \gamma_{a2}\Big(1 - \Gamma(x,t)\Big)(E(x,t) - E_T(t)), \tag{5}$$

where D_E represents the nutrient diffusion coefficient in the algae biofilm along the x direction, K_a is the half-saturation constant, and γ_{a1}, γ_{a2} are parameters controlling the nutrient uptake and inflow rates, respectively. Notice that the uptake rate constant γ_{a1} might depend on the concentration of algal cells within the biofilm and their affinity for the nutrient [27]. Different operating conditions for light, rotation, and nutrients are expected to result in biofilms with different (dry) algal biomass and, thus, different uptake constants. Meanwhile, the intake constant γ_{a2} might depend on the bioreactor's geometry, hydrodynamics, and reaction kinetics. Here we assume γ_{a1} and γ_{a2} as constants for simplicity.

The overall nutrient availability $E_T(t)$ in the wastewater is described by

$$\partial_t E_T(t) = \frac{S}{V} \int_0^L \gamma_{a2}\Big(1 - \Gamma(x,t)\Big)\Big(E(x,t) - E_T(t)\Big)dx, \tag{6}$$

with S the surface area of the substratum in the RABR, V the wastewater tank volume, and γ_{a2} the nutrient intake rate from the water to the RABR. We emphasize that when there is no nutrient consumption by the algae biofilm, i.e., when $\gamma_{a1} = 0$, the nutrient mass balance is respected by the model as

$$\frac{d}{dt}\Big(E_T(t)V + S\int_0^L E(x,t)dx\Big) = 0.$$

This study only considers the stratification in photosynthetic activity, which is the primary factor for algae biofilm growth. Another important factor is the vertical stratification of nutrients as steep chemical gradients may develop even at small length scales and thin biofilms, depending on the flow regime, the nutrient diffusivity, the concentration and uptake rate of the algal cells [27] and the coupled stratification in light intensity and nutrient concentrations may, in turn, induce algal mixotrophy [28,29]. And eq. (5) and eq. (6) are only valid for small spatial and slow temporal variations in the biofilm thickness. These aspects will be further investigated in our later work.

2.4. Water evaporation mechanism

Next, we introduce the model for water evaporation from the algae biofilm. We use $W(x,t)$ to represent the water saturation percentage. The dynamic behavior $W(x,t)$ is governed by the equation

$$\partial_t W(x,t) = D_W W_{xx} - \gamma_{w1}\Gamma(x,t)\frac{W(x,t)}{K_W + W(x,t)} + \gamma_{w2}\Big(1-\Gamma(x,t)\Big)\Big(1-W(x,t)\Big), \tag{7}$$

where D_W is the diffusion coefficient of water saturation along the x direction of the algae biofilm, γ_{w1} is the rate of water evaporation and γ_{w2} represents the absorbing rate from the wastewater. We assume it as a constant for simplicity, but it could also depend on the temperature and moisture of the air in certain situations.

In our study, the primary focus is on the impacts of water evaporation on algae biofilm growth since the RABR is rotating slowly. However, we note that the hydrodynamic conditions within the RABR system will have impacts on algae biofilm formation and stability. For instance, the shear stress would affect the architecture and cohesion of microalgae biofilms [30]. At low shear, the biofilms exhibited stratification in cohesion and were prone to detachment. By contrast, higher shear resulted in more stable and thicker biofilms. Interested readers can refer to [27,31–34] for modeling biofilm mechanics and detachment. These factors could be further considered to expand the current model.

2.5. Algae biofilm thickness and growth dynamics

Now, we are ready to introduce the algae biofilm thickness and growth dynamics under the effect of light attenuation, nutrient availability, and water evaporation. Denote the algae biomass concentration as $\phi(x,t)$ measured in g/m^2. Utilizing the photosynthetic activity illustrated in Fig. 3, the growth rate of the algae biofilm is expressed as [18]:

$$\partial_t \phi(x,t) = \Big[\frac{1}{h(x,t)}\int_0^{h(x,t)}\Big(k\frac{B(x,z,t)}{\tau} - R(x,z,t)\Big)dz\Big]\phi(x,t), \tag{8}$$

where $h(x,t)$ is the thickness of the biomass, $R(x,z,t)$ represents the respiration rate, and k is a growth rate constant that is determined with empirical studies of algae biofilm growth rates in laboratory settings. This paper assumes a constant respiration rate $R(x,z,t) = R$ for simplicity.

To simplify the model and given that the algae biofilm is usually thin, we assume the uniform density of the algae biofilm at various heights, with ρ representing the algae biofilm's areal dry biomass density, leading to the relationship between concentration and biomass thickness as

$$\phi(x,t) = \rho h(x,t), \tag{9}$$

where $h(x,t)$ denote the algae biofilm height. This simplification yields the growth equation for biofilm thickness

$$\partial_t h(x,t) = \int_0^{h(x,t)} k\frac{B(x,z,t)}{\tau}dz - Rh(x,t). \tag{10}$$

Adding the effects of spatial diffusion, nutrient limitation, and the constraints due to water evaporation, we finally obtain the complete version equation for algae biofilm growth as

$$\partial_t h(x,t) = D_h h_{xx} + \int_0^{h(x,t)} \frac{kB(x,z,t)}{\tau}\frac{E(x,t)}{K_a + E(x,t)}\frac{W(x,t)}{K_W + W(x,t)}dz - \Big(R + \frac{R_W K_W}{W(x,t)+K_W}\Big)h(x,t),$$

where D_h is the diffusion coefficient of algae biofilm height along the x direction, K_W denotes the critical threshold for water stress affecting algae biofilm growth, and R_W is the additional mortality rate under water stress. The term $\frac{W(x,t)}{K_W+W(x,t)}$ quantifies the impact of water stress on algal biofilm growth at location x, and $\frac{K_W}{W(x,t)+K_W}$ accounts for the influence of water stress on algal biofilm mortality.

Table 1
Parameter table with fixed parameter values.

Symbol	Value	Units	Description
σ	1.9×10^{-3}	$m^2\ \mu mol^{-1}$	effective absorption rate
t_0	0	s	start of time period of simulated algae biofilm growth
τ	6.849	s	turnover time of the electron transport chain
k_d	2.99×10^{-4}	s^{-1}	damage rate
k_r	4.8×10^{-4}	s^{-1}	repair rate
R	0.12	d^{-1}	respiration rate
b	1400	m^{-1}	light attenuation factor
ρ	140000	gm^{-3}	dry algae biomass density
p	6	-	number of simulated layers of algal biofilms
C_0	0.2	-	initial value for C state
K_W	0.5	-	critical threshold for water stress
γ_{w1}	2.5×10^{-3}	s^{-1}	rate of evaporation
γ_{w2}	1	s^{-1}	rate of water absorption
γ_{a2}	1	s^{-1}	rate of nutrient absorption
R_W	0.12	d^{-1}	water stress on algal biofilm death
D_A, D_B, D_C, D_h	10^{-6}	m^2s^{-1}	diffusion constant for algae biofilms
D_E	10^{-9}	m^2s^{-1}	diffusion constant of E amongst spatial element x
D_W	10^{-4}	m^2s^{-1}	diffusion constant of W amongst spatial element x

2.6. Governing equations and parameters

Overall, we summarize the proposed model as below

$$
\begin{cases}
\partial_t h(x,t) = D_h h_{xx} + \displaystyle\int_0^{h(x,t)} k\frac{B(x,z,t)}{\tau}\frac{E(x,t)}{K_a+E(x,t)}\frac{W(x,t)}{K_W+W(x,t)}dz - \Big(R+\frac{R_W K_W}{W(x,t)+K_W}\Big)h(x,t),\\
\partial_t B(x,z,t) = D_B B_{xx} + \sigma I(x,z,t) - \sigma I(x,z,t)C(x,z,t) - \Big(\sigma I(x,z,t) + k_d\sigma I(x,z,t) + \frac{1}{\tau}\Big)B(x,z,t),\\
\partial_t C(x,z,t) = D_C C_{xx} - k_r C(x,z,t) + k_d\sigma I(x,z,t)B(x,z,t),\\
\partial_t E(x,t) = D_E E_{xx} - \gamma_{a1}\frac{E(x,t)}{K_a+E(x,t)}\displaystyle\int_0^{h(x,t)} B(x,z,t)dz - \gamma_{a2}\Big(1-\Gamma(x,t)\Big)(E(x,t)-E_T(t)),\\
\frac{dE_T(t)}{dt} = \frac{S}{V}\displaystyle\int_0^{L}\gamma_{a2}\Big(1-\Gamma(x,t))(E(x,t)-E_T(t)\Big)dx,\\
\partial_t W(x,t) = D_W W_{xx} - \gamma_{w1}\Gamma(x,t)\frac{W(x,t)}{K_W+W(x,t)} + \gamma_{w2}\Big(1-\Gamma(x,t)\Big)\Big(1-W(x,t)\Big),
\end{cases}
\tag{11}
$$

where $x\in[0,L)$ and $z\in[0,h(x,t)]$. The periodic boundary condition is used for the x-direction.

To better present the parameter choices, we summarize all our model parameters in three tables, representing three types of model parameters. First, some model parameters can be fixed based on existing literature [18,25,35–37]. These parameters are summarized in Table 1.

Secondly, some parameters are based on realistic design parameters. These are summarized in Table 2. We elaborate on the decisions for some parameters in Table 2. The volume V has been selected such that the volume-to-surface area ratio between the RABR media and substratum is 50:1. k has been chosen as 0.00015 such that the resultant productivity values reflect those in existing literature [7]. γ_a has been selected such that the algae biofilm will experience inhibition in growth if not replenished within approximately 8 hours. γ_T has been chosen such that in laboratory conditions, the nutrient concentration of the media within the system will be below K_a after 72 hours [25].

In addition, parameters with undetermined values are summarized in Table 3. These are operation parameters for RABR. One of the goals of this paper is to investigate these operation parameters, discover their correlations, and understand how these operational conditions would affect biomass productivity. Their values will be specified in the corresponding numerical examples.

2.7. Harvesting strategies

As the algae biofilm grows in height, the depth of the algae biofilm will prevent algae on the bottom layers from receiving sufficient light, eventually leading to a stagnation of growth. To mitigate this stagnation and to maximize productivity, regular harvesting of the algae biofilm occurs in both laboratory and industrial settings to reduce the algae biofilm height. Ultimately, the goal is to increase biomass productivity.

Table 2
Parameter table with experimental parameter values.

Symbol	Value	Units	Description
S	1	m^2	surface area of the substratum in the RABR
h_0	0.0005	m	initial height of algae biofilm
L	7	m	circumference of the substratum in the RABR
l^*	3	m	arc length of the RABR exposed to air
v	0.1555	ms^{-1}	peripheral velocity of the RABR
T	45	s	period of the RABR's rotation
V	50	L	volume of the tank of the RABR
k	0.00015	-	growth rate
γ_{a1}	1575	$gm^{-2}d^{-1}$	rate of the algae biofilm nutrient consumption
K_a	1	mgL^{-1}	half-saturation constant for nutrient

Table 3
Parameter table with undetermined parameter values.

Symbol	Units	Description
$\hat{I}(t)$	$\mu mol m^{-2}s^{-1}$	light intensity
v	ms^{-1}	peripheral velocity of the RABR
h_a	m	residual height of algae biofilm after each harvest
$t_{harvest}$	s	time lags between consecutive algae biofilm harvests

Within the context of algae biofilm harvesting, there are two primary parameters to study. The first is the harvesting frequency, labeled as v; the second is the residual height of harvesting, marked as $h_a(x)$. When performing a harvest, no harvest will occur if the algae biofilm height is less than $h_a(x)$; otherwise, the algae biofilm is harvested with a thickness of $h_a(x)$ left. Intuitively, algae biofilm harvested too infrequently will experience light-limited stagnation, and algae biofilm harvested too often will limit biomass growth and cost more energy. Additionally, when harvesting the algae biofilm, consideration must be made of how much algae biofilm to remove. When $h_a(x)$ is large, much of the algae biofilm will remain after a harvest, implying harvesting will often occur to maintain a certain height. When $h_a(x)$ is small, a harvest will remove most of the algae biofilm and imply fewer, more extreme harvests.

To explore the spatial heterogeneity of our proposed model in eq. (11), we will test several heterogeneous harvesting strategies along the spatial variable x. Specifically, we will examine four strategies: (a) uniform harvest strategy, (b) checker harvest strategy, (c) linear harvest strategy, and (d) quadratic harvest strategy. To detail each strategy, we divide the substratum of length L into N equal meshes, marking the mesh points as x_j where $j = 0, 1, \ldots, N-1$. For the uniform harvest strategy, the post-harvest algae biofilm thickness is defined as

$$h(x) = \min(h(x), h_a(x));$$

for the checker harvest strategy, it is updated according to

$$h(x_j) = \begin{cases} \min(h(x_j), h_a(x_j)), & \text{if } j \pmod 2 = 0, \\ h(x_j), & \text{if } j \pmod 2 = 1, \end{cases}$$

after each harvest; for the linear harvest strategy, the post-harvest algae biofilm height is modified as

$$h(x) = (1 - \frac{x}{L}) \min(h_a(x), h(x)) + \frac{x}{L} h(x);$$

and for the quadratic harvest strategy, it is updated as

$$h(x) = 4\left(1 - \frac{x}{L}\right)\frac{x}{L} h(x) + \left(1 - 4\left(1 - \frac{x}{L}\right)\frac{x}{L}\right) \min\left(h_a(x), h(x)\right).$$

The four harvesting strategies are depicted in Fig. 5.

2.8. Numerical methods

The mathematical model proposed in eq. (11) is a free surface problem. The periodic boundary condition is used for the x-direction as the substratum rope forms a closed loop. It is a coupled system with integral differential equations. To solve eq. (11) numerically, we discretize the spatial domain $x \in [0, L)$ into uniform meshes

$$0 < x_1 < x_2 < \cdots < x_N < L,$$

where

$$x_j = (j - 0.5)\delta_x, \quad \delta_x = \frac{L}{N}, \quad j = 1, \cdots, N.$$

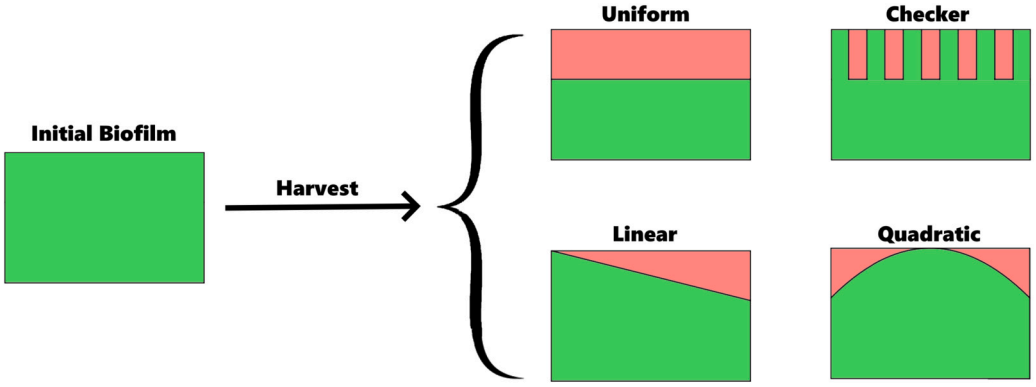

Fig. 5. A schematic illustration of various harvesting strategies. The areas shaded in red represent the mass that will be removed following the corresponding harvest strategy. The residual algae biofilm height, i.e., the minimum height that will be considered for removal during a harvest, is set with $h_a(x)$.

Next, we partition the algae biofilm depth domain $[0, h(x_j,t)]$ into p intervals:

$$0 \le z_1(x_j,t) < z_2(x_j,t) < \cdots < z_p(x_j,t) < h(x_j,t), \quad z_i(x_j,t) = \frac{i-1}{p} h(x_j,t).$$

By approximating the dynamics with p layers and N segments, we obtain the following system of differential equations to represent the dynamics in each layer and each section:

$$\begin{cases} \frac{d}{dt}h_j = D_h \frac{h_{j+1} - 2h_j + h_{j-1}}{\delta_x^2} + \sum_{i=1}^{p} \frac{h_j}{p} k \frac{B_{ij}}{\tau} \frac{E_j}{K_a + E_j} \frac{\frac{3}{2}W_j}{K_W + W_j} - \left(R + R_W \frac{K_W}{W_j + K_W}\right) h_j, \\ \frac{d}{dt}B_{ij} = D_B \frac{B_{i,j+1} - 2B_{ij} + B_{i,j-1}}{\delta_x^2} + \sigma I_{ij}(t) - \sigma I_{ij}(t) C_{ij} - \left(\sigma I_{ij}(t) + k_d \sigma I_{ij}(t) + \frac{1}{\tau}\right) B_{ij}, \\ \frac{d}{dt}C_{ij} = D_C \frac{C_{i,j+1} - 2C_{ij} + C_{i,j-1}}{\delta_x^2} - k_r C_{ij} + k_d \sigma I_{ij}(t) B_{ij}, \\ \frac{d}{dt}E_j = D_E \frac{E_{j+1} - 2E_j + E_{j-1}}{\delta_x^2} - \gamma_{a1} \frac{E_j}{K_a + E_j} \frac{h_j}{p} \sum_{i=1}^{p} B_{ij} - \gamma_{a2}\left(1 - \Gamma_j\right)(E_j - E_T), \\ \frac{d}{dt}E_T = \frac{S}{VN} \sum_{j=0}^{N-1} \gamma_{a2} h_j (1 - \Gamma_j)(E_j - E_T), \\ \frac{d}{dt}W_j = D_W \frac{W_{j+1} - 2W_j + W_{j-1}}{\delta_x^2} - \gamma_{w1} \Gamma_j \frac{W_j}{K_W + W_j} - \gamma_{w2}\left(1 - \Gamma_j\right)\left(W_j - 1\right), \end{cases} \tag{12}$$

where $i = 1, 2, \cdots, p$ and $j = 1, 2, \cdots, N$. In eq. (12), $B_{ij}(t)$ and $C_{ij}(t)$ represent the value at (z_i, x_j), and the light intensity at the ith layer and jth section is approximated by

$$I_{ij}(t) = \frac{p}{h(x_j,t)} \int_{z_i}^{z_{i+1}} I(x_j,t) e^{-b(h(x_j,t)-z)} dz, \quad i = 1, 2, \cdots p, \quad j = 1, 2, \cdots N.$$

Given the periodic boundary condition is used for the x-direction, we have the following

$$B_{iN+1} = B_{i1}, C_{iN} = C_{i1}, B_{i0} = B_{iN}, C_{i0} = C_{iN}.$$

The semi-discrete model in equation (12) is a coupled ODE system. To simplify the notations, we denote the ODE system in eq. (12) as

$$\begin{cases} \frac{d}{dt}\Phi(t) = F(\Phi(t)), \\ \Phi(0) = \Phi_0, \end{cases} \tag{13}$$

with F the reactive kinetics and Φ is a vector notation for the unknowns. The problem in eq. (13) is solved by an implicit method based on the variable order backward-differentiation formula [38], as implemented in the python SciPy package, and a time step $\delta t = 0.1$ second is used.

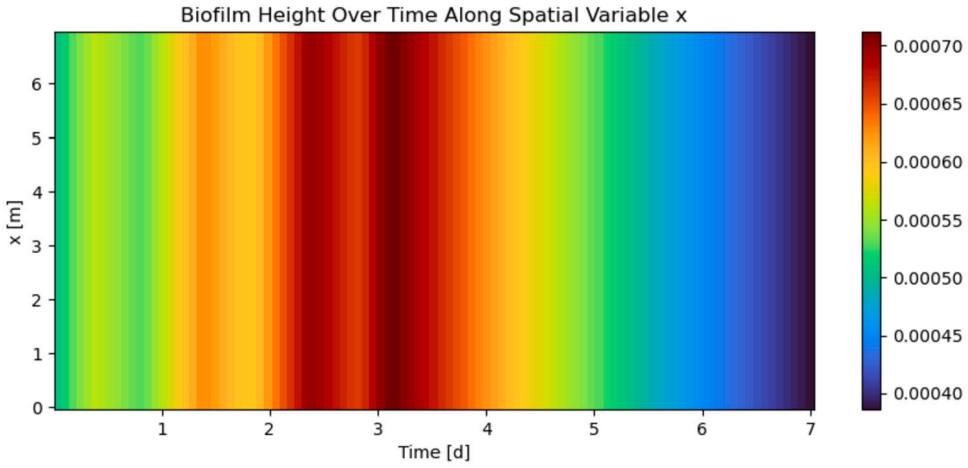

Fig. 6. Algae biofilm thickness over time. This figure displays the algae biofilm height along the spatial variable x over a seven-day simulation within a nutrient-limited environment. On Day 3, the nutrient in the wastewater depletes and stalls algae biofilm growth.

We initialize our values of A, B, and C by $(A_0, B_0, C_0) = \left(\frac{1-C_0}{1+\tau\sigma I}, \frac{\tau\sigma I(1-C_0)}{1+\tau\sigma I}, C_0\right)$, making it compatible with the steady-state solution of the model in [18]. Here, C_0 is a hyper-parameter indicating the proportion of cells in an inhibited state. Since the initial state is unknown, we assume $C_0 = 0.2$ for all our numerical simulations. A detailed investigation of the effect of C_0 will not be elaborated. Also, $N = 15$ is picked in the numerical simulations unless otherwise specified.

3. Results

Several simulations were conducted to explore the inclusion of empirical PPFD values and the spatial variable x for our model. Otherwise specified, the parameters used to produce these figures are taken from the parameter tables in the previous section. For all simulations utilizing the real PPFD values in Fig. 4, we use $t = 8$ hours for the data at the beginning of the simulation to mimic a start at 8:00 AM for the PPFD.

3.1. Algae biofilm growth in a nutrient-limited environment

For the first numerical study, we perform a seven-day simulation in a nutrient-limited setting using the light data presented in Fig. 4. The simulation results are summarized in Fig. 6. The algae biofilm height oscillates following the diurnal cycle of the photosynthetic photon flux density (PPFD) light data shown in Fig. 4. During daylight hours, as indicated in Fig. 4, the PPFD is high, promoting biomass growth. Conversely, with PPFD at 0 $\mu mol m^{-2}s^{-1}$ overnight, there is no biomass growth, and the dynamics of the algae biofilm are primarily governed by cellular respiration. As shown in Fig. 6, the biofilm undergoes net growth from $0 < t < 3$ days. However, by approximately $t = 3$ days, the nutrient in the wastewater, E_T, depletes to 0 mg/L, limiting further growth of the algae biofilm. The lack of nutrients in the wastewater from $t = 3$ days onwards leads to a net reduction in biomass for all substratum locations. The numerical results indicate that our proposed model can capture the dynamics effectively.

Fig. 7 depicts the nutrient concentration of Fig. 6 over time. In the short time period, as shown in Fig. 7(a), one can notice the nutrient concentration in the algae biofilms, E, fluctuates periodically, accurately mirroring the RABR's rotation in and out of the wastewater. Concurrently, the nutrient concentration in the wastewater, E_T, gradually decreases, indicative of nutrient consumption by the algae biofilm. Over an extended one-day period, as illustrated in Fig. 7(b), the nutrient concentrations in both the algae biofilm and wastewater are consistent, with the concentration in the algae biofilm being marginally lower. For every day, as Fig. 7(c) demonstrates, nutrient consumption occurs rapidly during daylight hours and stalls at night due to the absence of sunlight. This figure further validates that our proposed model can accurately capture the dynamics of nutrient depletion over time.

3.2. Algae biofilm growth with a RABR deactivation

In the next study, we conduct a seven-day simulation to emulate a malfunction or maintenance scenario in the RABR. Initially, the algae biofilm is in a nutrient-rich environment. From Day 0 to Day 3, the algae biofilm's state is similar to that depicted in Fig. 6, exhibiting homogeneity across the spatial variable x. On Day 3, a mechanical malfunction occurs, halting the RABR's rotation ($v = 0$ m/s) for 24 hours. During this period, part of the algae biofilm remains in the air regime ($\Gamma(x,t) = 1$), while the rest is in the water regime ($\Gamma(x,t) = 0$). Recall our parameter selection in Table 2, 3 meters of the substratum are exposed to the air and 4 meters to the wastewater.

At $t = 3$ days, $\Gamma(x,t) = 0$ for $0 < x < 4$. In this stalled phase, the differences in biofilm growth and decay mechanisms between the water and air regimes become more pronounced. The biofilm in the water regime ($0 < x < 4$) for $t = 3$ days experiences no growth due to the absence of photosynthetic photon flux density (PPFD) and gradually diminishes, influenced by cellular respiration and

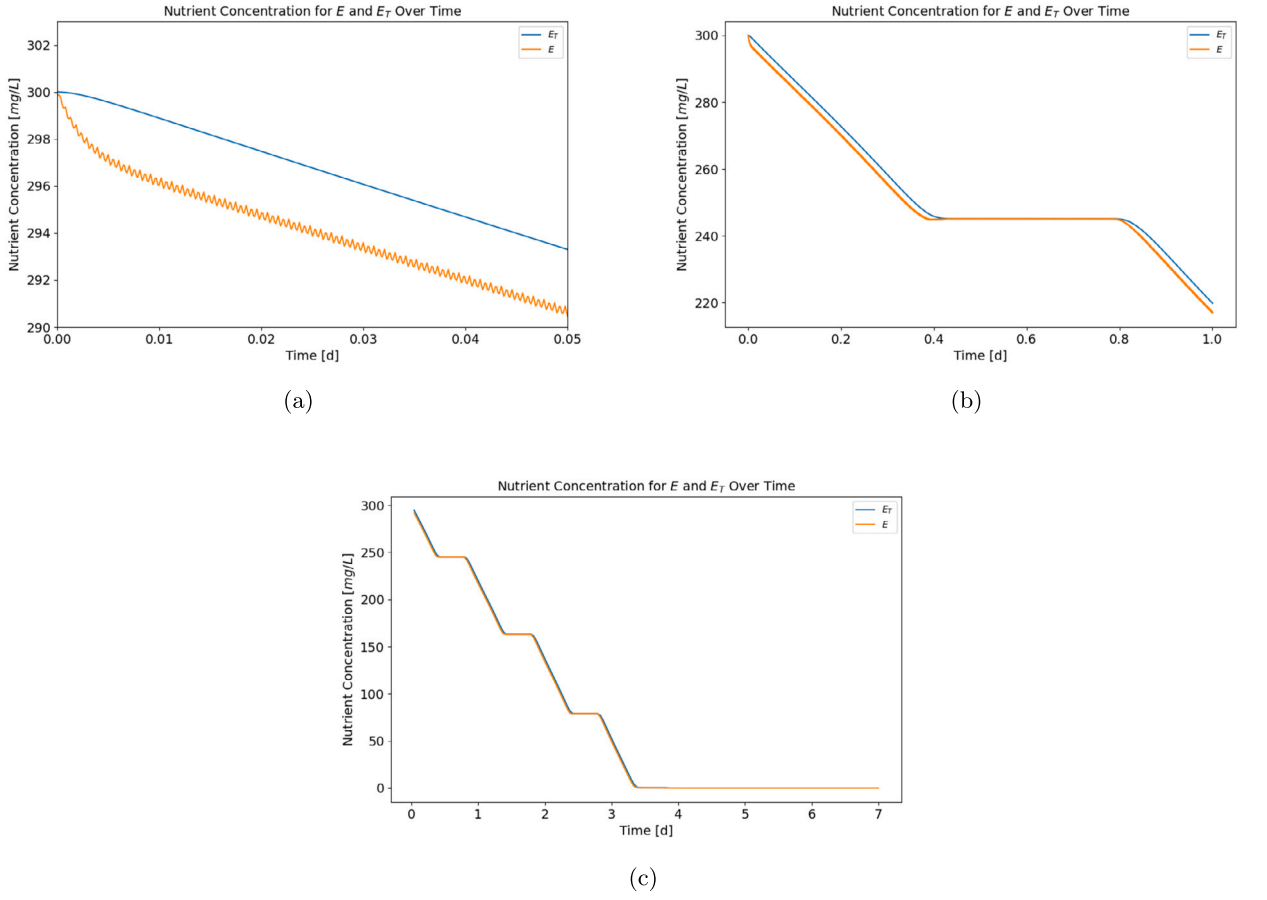

Fig. 7. Nutrient depletion over time. This figure illustrates (a) the nutrient concentration over a short period, (b) the nutrient concentration over a one-day period, and (c) the nutrient concentration over a long period. In the figure, both the nutrient in the algae biofilm $E(t) := E(0,t)$ and the averaged nutrient in the wastewater $E_T(t)$ are visualized.

metabolism. Conversely, the biofilm in the air regime for $t = 3$ days ($4 < x < 7$), although exposed to PPFD, suffers from accelerated nutrient depletion and water evaporation. The stress is more severe in the air regime, leading to a heterogeneous biofilm distribution along x. On Day 4, the RABR is repaired and resumes normal rotation. During the remaining simulation days, the algae biofilm gradually recovers and is approximately homogeneous again by $t = 7$ days.

The biofilm heights on Day 3 and Day 4 are visualized in Fig. 9. As we can tell from Fig. 9(a), the algae biofilm is roughly homogeneous on Day 3. This is due to the continuous rotation of the RABR in and out of the wastewater on a faster time scale. The algae biofilm at different locations of the substratum has equal access to the nutrients from the wastewater. However, due to the RABR's halted rotation, the algae biofilms in the air and wastewater experience different stress, leading to a heterogeneous distribution on Day 4, as illustrated in Fig. 9(b).

In the remainder of this paper, we simulate the algae biofilm growth in a nutrient-rich environment. This is achieved by replacing the wastewater in the container every two days during long-time simulations. This approach is designed to mimic the scenario in which the wastewater retention time is two days.

3.3. Impact of the harvesting patterns on biomass productivity

Next, we investigate the impact of non-homogeneous harvesting strategies on the height and productivity of algae biofilm. The algae biofilm yield is defined as the net growth in the RABR with the unit g/m^2, which includes the biomass harvested and the portion remaining in the RABR. The productivity P of the algae biofilm for the upcoming simulations is calculated by dividing the yield of the algae biofilm by the elapsed time and the total surface area of the substratum, i.e.,

$$P := \frac{\text{yield of algae biofilm}}{\text{elapsed time}},$$

with the unit $g/(m^2 d)$. We will explore five strategies: no harvesting, uniform harvesting, checker harvesting, linear harvesting, and quadratic harvesting. The details for the harvesting strategies are presented in the previous section, with a summary shown in Fig. 5.

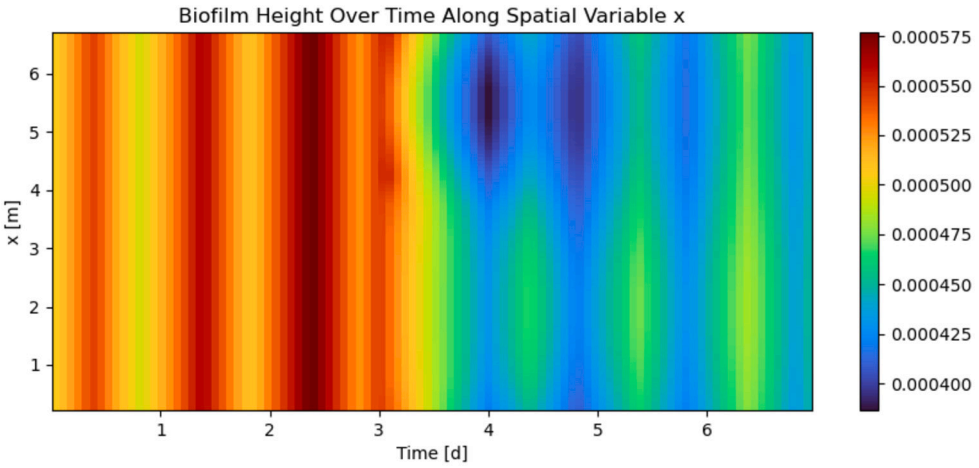

Fig. 8. Alage biofilm thickness over time. This figure displays the algae biofilm height along the spatial variable x over a seven-day simulation in which $v = 0$ between days 3 and 4. The lack of spinning creates a heterogeneous algae biofilm and recovers into a more homogeneous structure after day 4. We have used $N = 14$ for this simulation.

Table 4
Productivity of selected harvest strategies.

Strategy	Productivity g/m^2d
No Harvest	2.2277
Uniform Harvest	2.1713
Checker Harvest	2.1981
Linear Harvest	2.2000
Quadratic Harvest	2.2066

To better compare different harvesting patterns, we present a control simulation with no harvesting on the algae biofilm, given in Fig. 10.

Fig. 11 summarizes the numerical results with various harvesting strategies, with a harvest executed at $t = 2$ days and a residual depth $h_a = 0.0005m$. Before harvesting, for $0 < t < 2$ days, the algae biofilm heights within all subfigures of Fig. 11 align with that in Fig. 10. Following the harvest at $t = 2$ days, the algae biofilm becomes heterogeneous along the spatial variable x for the checker, linear, and quadratic harvesting strategies. However, within 48 hours of the post-harvest period, the algae biofilms in each harvesting strategy become homogeneous again along x. Among these strategies, the checker harvest leads to the quickest homogenization of the algae biofilm, followed by the quadratic and linear harvests, as indicated in Fig. 11. This uniform recovery of the algae biofilm post-harvest is attributed to the RABR's consistent rotation, which ensures equal and adequate nutrient distribution.

The productivity results at $t = 4$ days are presented in Table 4 for a comprehensive comparison of the harvesting strategies. An analysis of these results suggests that, given the parameters used in Fig. 11, $\nu = 2$ days is too frequent to benefit algae biofilm growth. Notably, the strategy yielding the highest algae biofilm productivity was to avoid harvesting altogether, resulting in productivity of $2.2277 g/(m^2 d)$ when considering the total biomass yield over the 4-day period. Among the strategies that involved harvesting, the one removing the least amount of algae biofilm, the quadratic harvesting strategy, achieved productivity of $2.2066 g/(m^2 d)$. Conversely, the strategy that harvested the most algae biofilm at $t = 2$ days, the uniform harvesting strategy, resulted in a lower productivity of $2.1713 g/(m^2 d)$. In other words, the more biomass removed at $t = 2$ days, the lower the resulting productivity from the simulations depicted in Fig. 11. This indicates that harvesting frequency would impact biomass productivity, which we will explore later in this paper.

3.4. Influence of light exposure and light intensity on biomass productivity

Next, we investigate the impact of light on biomass productivity, considering two scenarios: altering maximum light intensity and changing the ratio of substratum exposure to air in the RABR.

In the first scenario, we introduce the parameter γ to modify the maximum light intensity, namely replacing $\hat{I}_0(t)$ in eq. (3) by $\gamma \hat{I}_0(t)$. The numerical predictions for biomass productivity over a 4-day period are summarized in Fig. 12(a). The results reveal that excessively strong and weak light conditions decrease biomass productivity. This finding underscores the necessity of optimal light management, potentially involving light filters for overly intense light or artificial lighting in low-light conditions. Note that the energy efficiency of artificial lighting should also be considered in such cases.

In the second scenario, we investigate the impact of varying r_0, the ratio of substratum exposed to air, while other factors remain fixed. The numerical outcomes are illustrated in Fig. 12(b). This figure indicates that a higher percentage of substratum exposed to the air benefits the algae biofilm productivity. However, there is a threshold for productivity to decrease afterward. Prolonged

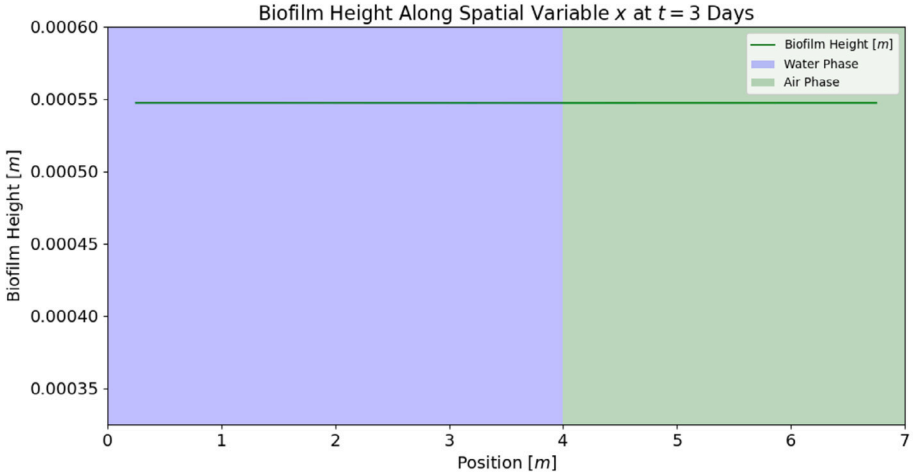

(a) Algae biofilm height at Day 3

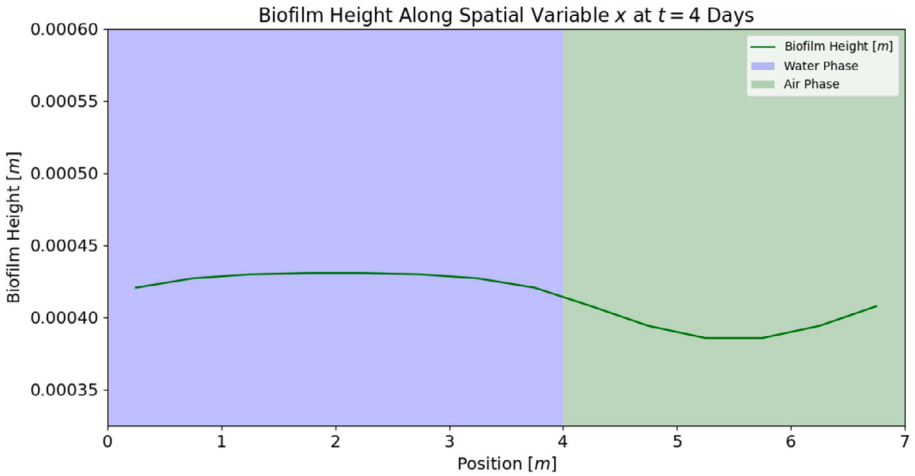

(b) Algae biofilm height at Day 4

Fig. 9. Algae biofilm height at Day 3 and Day 4 for the study in Fig. 8.

exposure of the substratum to air would ensure the algae biofilm has sufficient exposure to the sunlight for photosynthesis, thus increasing biomass productivity. However, if an excessive percentage of substratum is exposed to the air, it would lead to insufficient contact time for the substratum in the wastewater, which is essential for absorbing nutrients necessary for biomass production. Therefore, finding an optimal balance in substratum exposure to sunlight and wastewater is critical.

3.5. Influence of harvesting frequency on biomass productivity

To explore the impact of different harvesting frequencies on biomass productivity, we conducted four 56-day simulations with varying harvest intervals (ν): 1 day, 2 days, 3.5 days, 7 days, 14 days, and 28 days. We employed the checker harvesting strategy for these simulations and chose a residual algae biofilm thickness of $h_a = 0.0005m$. The results of $\nu = 1, 2, 3.5$ and 7 are illustrated in Fig. 13. The outcomes indicate that excessive harvesting may prevent the algae biofilm from attaining greater thickness.

To quantitatively compare the results of different ν values shown in Fig. 13, we summarize the productivity results at $t = 56$ days in Table 5. In line with our findings from Table 4, the parameters selected for the simulations in Fig. 13 favor a less frequent harvesting approach than $\nu = 2$ days. Among the frequencies examined, a frequency of $\nu = 3.5$ days yielded the highest productivity at $11.4757 gm^{-2}d^{-1}$, while the least frequent harvest ($\nu = 28$ days) resulted in the lowest productivity of $3.1737 gm^{-2}d^{-1}$. However, Fig. 13 also shows that less frequent harvesting allows for more robust biomass growth. However, it does not necessarily lead to the highest biomass yield over an extended period. This is mainly because a thicker algae biofilm can block sunlight from penetrating the

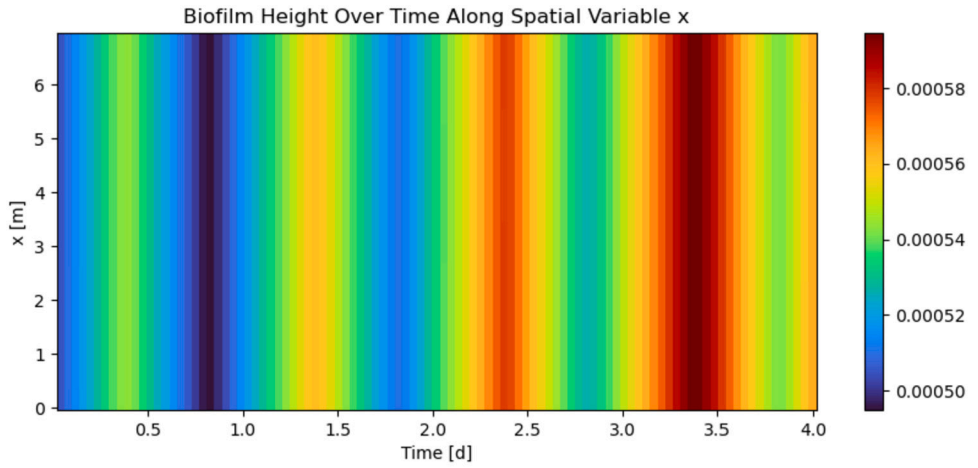

Fig. 10. Algae biofilm height along the spatial variable x over a four-day simulation. In this figure, the vertical axis represents the spatial location, and the horizontal axis represents the time. The algae biofilm resides in a nutrient-rich system, and no harvesting occurs. This is shown as a control compared to the results in later discussions.

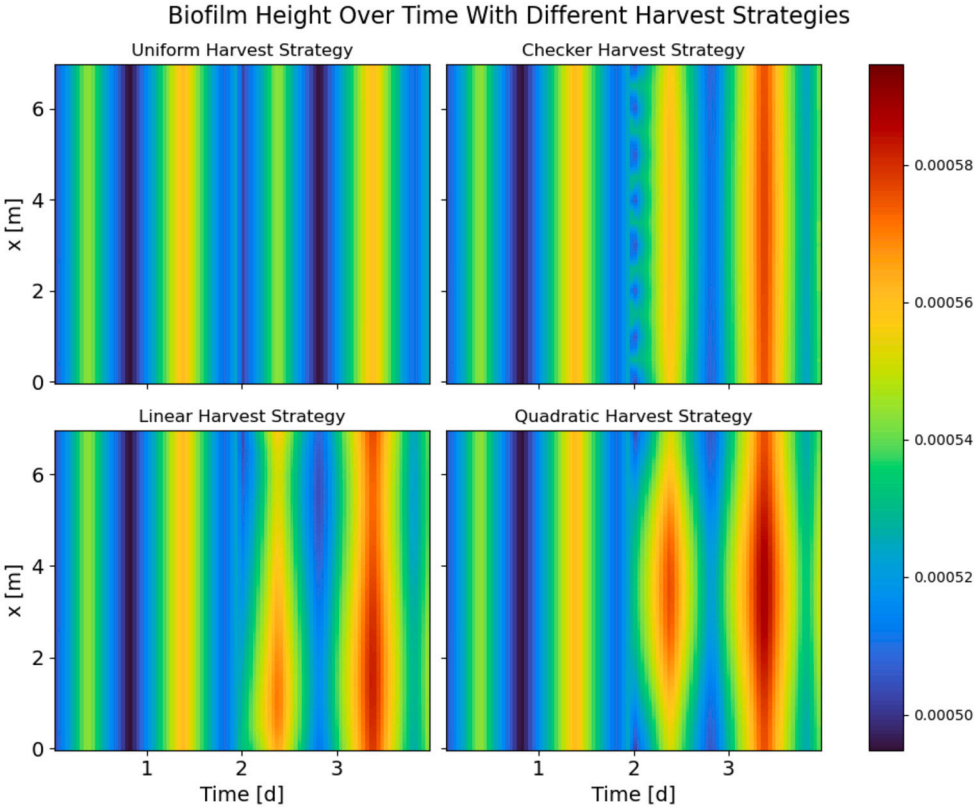

Fig. 11. A comparison of different harvesting strategies for the RABR over four-day simulations. At $t = 2$ days, a harvest is performed in each simulation. A different harvesting strategy is used in each subfigure in which $h_a(x) = 0.0005$ meters. See Methods for details on each harvesting strategy.

biomass near the substratum, thereby limiting biofilm growth. In summary, Table 5 suggests that a balance in harvesting frequency, i.e., neither too frequent nor too infrequent, is crucial for maximizing biomass productivity.

To better understand the effects of harvesting frequency on biomass yield and productivity, we further illustrate the results in Fig. 14. As shown in Fig. 14(a), more biomass is produced with $\nu = 3.5$ days, compared to the results for 1, 2, or 7 days over a long time. Additionally, productivity with $\nu = 7$ days is higher than other frequencies in the early stages but decreases over time. This indicates that an adaptive harvesting strategy could be beneficial; that is, the harvesting frequency should be adjusted based on other operating factors when sufficient laboratory data is available. Moreover, this numerical study further demonstrates the

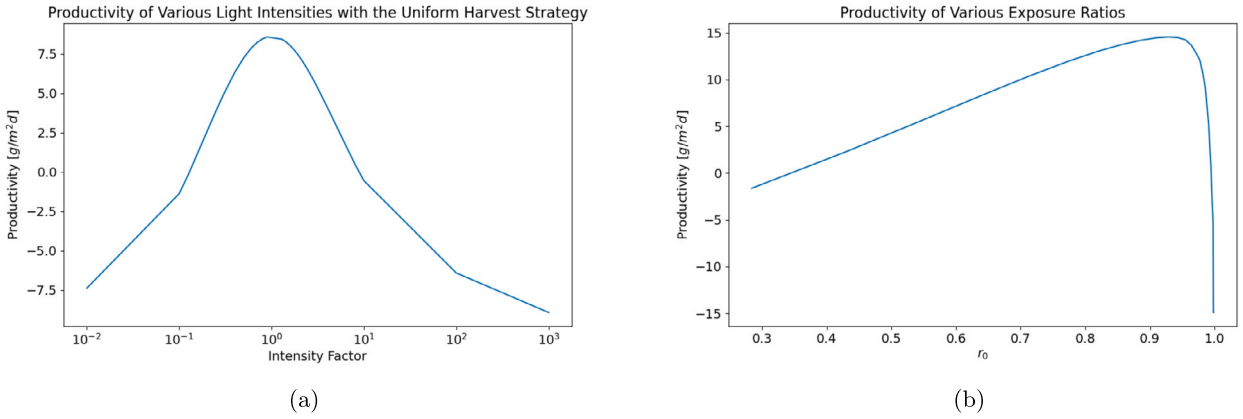

Fig. 12. Effects of light exposure and intensity on biomass productivity. This figure shows (a) the biomass productivity under various light intensities and (b) the biomass productivity with various ratios of substratum exposed to the air in the RABR.

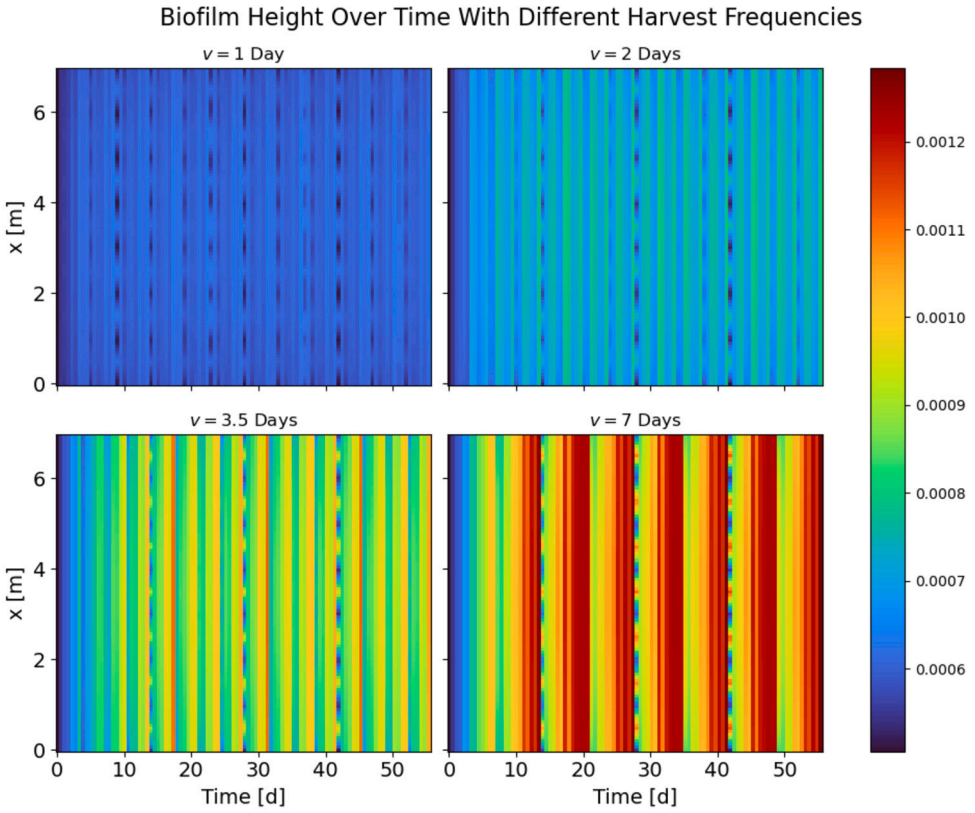

Fig. 13. This figure compares four harvesting frequencies in the RABR over a series of 56-day simulations. The checker harvest strategy is employed in each subfigure, with $h_a = 0.0005m$.

Table 5
Productivity of selected harvest frequencies.

Harvest Interval (v)	Productivity ($gm^{-2}d^{-1}$)
1 day	8.9858
2 days	10.4820
3.5 days	11.4757
7 days	8.1733
14 days	5.0884
28 days	3.1737

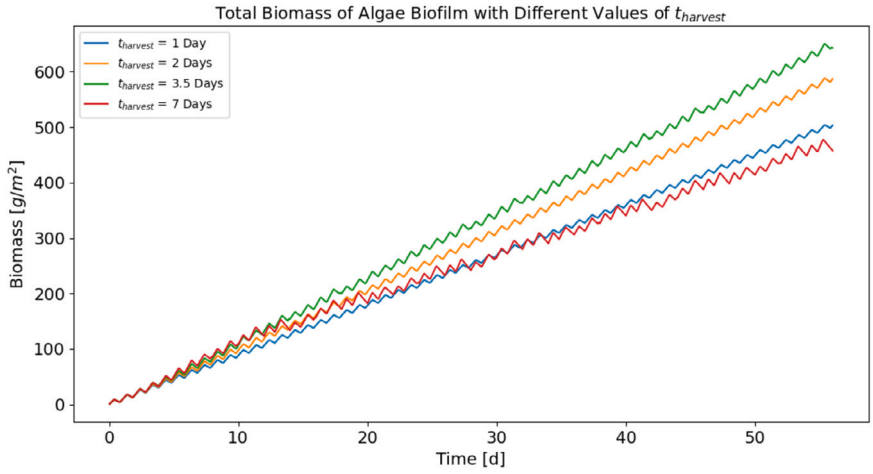

(a) Total biomass vs. time

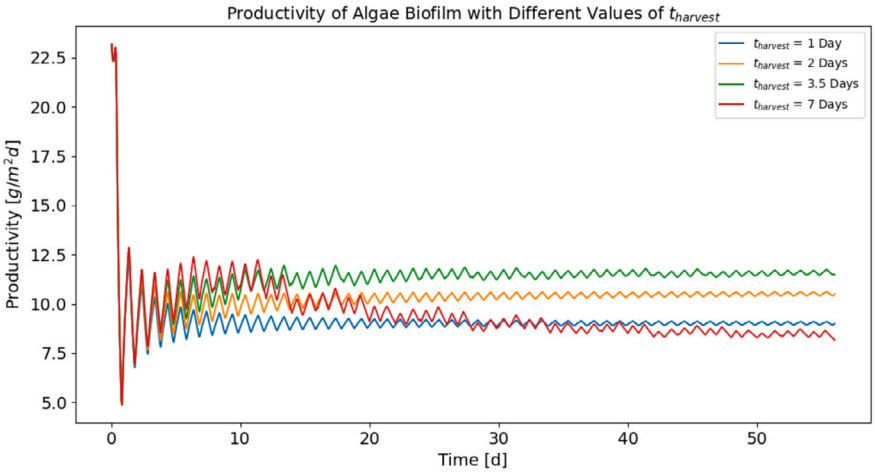

(b) Productivity vs. time

Fig. 14. Effect of harvesting frequency on biomass productivity. This figure shows (a) the total biomass produced at different harvesting frequencies and (b) the productivity across various harvesting frequencies over time.

approximation power of our proposed model and its ability to investigate optimal control and design of RABR to enhance biomass productivity and nutrient removal.

4. Conclusion

In this work, we have developed and presented a predictive mathematical model to investigate the complex growth dynamics of algae biofilms and the impacts of various environmental and operational factors on the algae biofilm productivity in the rotating algae biofilm reactors (RABRs). Our model considers both the photosynthetic mechanism and the spatial location across the substratum surface in the RABR, enabling a more accurate simulation of biofilm growth in RABRs. Our numerical study demonstrated its capabilities in studying the effects of the RABR's spatial heterogeneity on algae biofilm growth, offering valuable insights into the interplay between various environmental and operational factors and their influence on biomass productivity.

Our findings reveal that while biomass productivity does not vary significantly with different harvesting types, it is sensitive to the residual thickness of the algae biofilm left post-harvest. Both excessively thick and thin residual algae biofilm after harvesting can diminish productivity. Meanwhile, harvesting frequency also plays a crucial role. Overly frequent harvesting hurts biomass growth, while infrequent harvesting allows the development of a thick algae biofilm, which may reduce productivity due to limited sunlight penetration into the biomass closer to the substratum. Therefore, a balanced harvesting frequency is essential for optimal productivity. Moreover, our results indicate the importance of light management, as extreme sunlight conditions—either too strong

or too weak—can limit biomass production. Implementing a light shed or filter for intense light conditions and providing artificial lighting for low-light environments may increase biomass productivity. Additionally, the proportion of substratum exposure to air in the RABR significantly influences biomass production. The proposed mathematical model provides a theoretical framework for exploring and identifying the optimal environmental and operational parameters to enhance algae biofilm growth and increase biomass productivity in the RABR system for wastewater treatment.

Declaration of competing interest

The authors declare that they have no known competing financial interests or personal relationships that could have appeared to influence the work reported in this paper.

Data availability

No data was used for the research described in the article.

Acknowledgements

G. B. Jones and J. Zhao would like to acknowledge the support from the National Science Foundation (NSF) USA under grants DMS-1816783 and DMS-2111479. Ronald Sims would like to acknowledge the support from the U.S. Department of Energy EERE-Bioenergy Technologies Office (BETO) under Award EE0009271.

References

[1] I. Saadaoui, R. Rasheed, A. Aguilar, M. Cherif, H. Jabri, S. Sayadi, S. Manning, Microalgal-based feed: promising alternative feedstocks for livestock and poultry production, J. Animal Sci. Biotechnol. 12 (76) (2021).
[2] A. Ahmad, S.W. Hassan, F. Banat, An overview of microalgae biomass as a sustainable aquaculture feed ingredient: food security and circular economy, Bioengineered 13 (4) (2022) 9521–9547.
[3] P.K. Sharma, M. Saharia, R. Srivstava, S. Kumar, L. Sahook, Tailoring microalgae for efficient biofuel production, Front. Mar. Sci. 5 (2018).
[4] S. Zhang, L. Zhang, G. Xu, F. Li, X. Li, A review on biodiesel production from microalgae: influencing parameters and recent advanced technologies, Front. Microbiol. 12 (2022) 970028.
[5] S.G. Mastropetros, K. Pispas, D. Zagklis, S.S. Ali, M. Kornaros, Biopolymers production from microalgae and cyanobacteria cultivated in wastewater: recent advances, Biotechnol. Adv. 60 (2022) 107999.
[6] B. Ravindran, S.K. Gupta, W. Cho, J.K. Kim, S.R. Lee, K. Jeong, D.J. Lee, H. Choi, Microalgae potential and multiple roles—current progress and future prospects—an overview, Sustainability 8 (2016) 1215.
[7] L.B. Christenson, R.C. Sims, Rotating algal biofilm reactor and spool harvester for wastewater treatment with biofuels by-products, Biotechnol. Bioeng. 109 (7) (2012) 1674–1684.
[8] M. Kesaano, R.C. Sims, Algal biofilm based technology for wastewater treatment, Algal Res. 5 (2014) 231–240.
[9] K. Arora, P. Kaur, P. Kumar, A. Singh, S. Patel, X. Li, Y. Yang, S.K. Bhatia, S. Kulshrestha, Valorization of wastewater resources into biofuel and value-added products using microalgal system, Front. Energy Res. 9 (2021) 646571.
[10] A. Rahman, R.J. Putmana, K. Inan, F.A. Sal, A. Sathish, T. Smith, C. Nielsen, R.C. Sims, C.D. Miller, Polyhydroxybutyrate production using a wastewater microalgae based media, Algal Res. 8 (2015) 95–98.
[11] J.L. Wood, C.D. Miller, R.C. Sims, J.Y. Takemoto, Biomass and phycocyanin production from cyanobacteria dominated biofilm reactors cultured using oilfield and natural gas extraction produced water, Algal Res. 11 (2015) 165–168.
[12] K.M. Hillman, R.C. Sims, Struvite formation associated with the microalgae biofilm matrix of a rotating algal biofilm reactor (RABR) during nutrient removal from municipal wastewater, Water Sci. Technol. 81 (4) (2020) 644–655.
[13] J. Barlow, R.C. Sims, J.C. Quinn, Techno-economic and life-cycle assessment of an attached growth algal biorefinery, Bioresour. Technol. 220 (2016) 360–368.
[14] R. Sims, B. Peterson, Waste to value: algae-based biofuel utilizing oil and gas extraction wastewater, Acad. Lett. 4460 (2021) 12–21.
[15] S. Yang, A. Sathish, J. Eun, Y.M. Lee, V. Fellner, R.C. Sims, In vitro ruminal fermentation characteristics of algal protein precipitate supplemented in lactation dairy diets in continuous cultures, Int. J. Innov. Res. Sci. Eng. Technol. 8 (9) (2019) 9207–9218.
[16] Q. Béchet, A. Shilton, B. Guieysse, Modeling the effects of light and temperature on algae growth: state of the art and critical assessment for productivity prediction during outdoor cultivation, Biotechnol. Adv. 31 (8) (2013) 1648–1663.
[17] X. Wu, J.C. Merchuk, A model integrating fluid dynamics in photosynthesis and photoinhibition processes, Chem. Eng. Sci. 56 (2001) 3527–3538.
[18] O. Bara, H. Bonnefond, O. Bernard, Model development and light effect on a rotating algal biofilm, IFAC-PapersOnLine 52 (1) (2019) 376–381.
[19] B.E. Chalker, Modeling light saturation curves for photosynthesis: an exponential function, J. Theor. Biol. 84 (2) (1980) 205–215.
[20] J.J. Cullen, On models of growth and photosynthesis in phytoplankton, Deep-Sea Res., A, Oceanogr. Res. Pap. 37 (4) (1990) 667–683.
[21] C.D. Collins, C.W. Boylen, Physiological responses of Anabaena variabilis (Cyanophyceae) to instantaneous exposure to various combinations of light intensity and temperature, J. Phycol. 18 (2) (1982) 206–211.
[22] P. Eilers, J. Peeters, A model for the relationship between light intensity and the rate of photosynthesis in phytoplankton, Ecol. Model. 42 (3–4) (1988) 199–215.
[23] B. Polizzi, F. Andrea, F. Lopes, M. Ribot, O. Bernard, Understanding photosynthetic biofilm productivity and structure through 2D simulation, PLoS Comput. Biol. 18 (4) (2022) e1009904.
[24] G. Jones, D. Ellis, Z. Zhang, J. Zhao, R. Sims, Optimizing algae biofilm growth in wastewater treatment using predictive mathematical models, in: Contemporary Research in Mathematical Biology, World Scientific, 2023, p. 600.
[25] G. Jones, R. Sims, J. Zhao, Experimental and theoretical investigations of rotating algae biofilm reactors (RABRs): areal productivity, nutrient recovery, and energy efficiency, Biotechnol. Bioeng. 10 (2023) 2865–2879.
[26] R.J. Wicker, E. Kwon, E. Khan, V. Kumar, A. Bhatnagar, The potential of mixed-species biofilms to address remaining challenges for economically-feasible microalgal biorefineries: a review, Chem. Eng. J. 451 (2023) 138481.
[27] G.E. Kapellos, H.J. Eberl, N. Kalogerakis, P.S. Doyle, C.A. Paraskeva, Impact of microbial uptake on the nutrient plume around marine organic particles: high-resolution numerical analysis, Microorganisms 10 (2022) 2020.
[28] K.F. Edwards, Mixotrophy in nanoflagellates across environmental gradients in the ocean, Proc. Natl. Acad. Sci. USA 116 (13) (2019) 6211–6220.

[29] A. Tenore, M.R. Mattei, L. Frunzo, Modelling the ecology of phototrophic-heterotrophic biofilms, Commun. Nonlinear Sci. Numer. Simul. 94 (2021) 105577.
[30] A. Fanesi, M. Lavayssière, C. Breton, Shear stress affects the architecture and cohesion of chlorella vulgaris biofilms, Sci. Rep. 11 (2021) 4002.
[31] H. Gaebler, H. Eberl, A simple model of biofilm growth in a porous medium that accounts for detachment and attachment of suspended biomass and their contribution to substrate degradation, Eur. J. Appl. Math. 29 (6) (2018) 1110–1140.
[32] R. Sudarsan, S. Ghosh, J. Stockie, H. Eberl, Simulating biofilm deformation and detachment with the immersed boundary method, Commun. Comput. Phys. 19 (3) (2016) 682–732.
[33] J. Zhao, Y. Shen, M. Haapasalo, Z. Wang, Q. Wang, A 3d numerical study of antimicrobial persistence in heterogeneous multi-species biofilms, J. Theor. Biol. 392 (2016) 83–98.
[34] J. Zhao, Q. Wang, Three-dimensional numerical simulations of biofilm dynamics with quorum sensing in a flow cell, Bull. Math. Biol. 4 (2017) 884–919.
[35] B. Han, M. Virtanen, J. Koponen, M. Straškraba, Effect of photoinhibition on algal photosynthesis: a dynamic model, J. Plankton Res. 22 (5) (2000) 865–885.
[36] O. Bernard, B. Rémond, Validation of a simple model accounting for light and temperature effect on microalgal growth, Bioresour. Technol. 123 (2012) 520–527.
[37] B. Han, A mechanistic model of algal photoinhibition induced by photodamage to photosystem-II, J. Theor. Biol. 214 (4) (2002) 519–527.
[38] L.F. Shampine, M.W. Reichelt, The MATLAB ODE suite, SIAM J. Sci. Comput. 18 (1997) 1–22.